Published in final edited form as:
Anal Chem. 2010 April 1; 82(7): 2989–2995. doi:10.1021/ac100036p.

Sensitive Immunosensor for Cancer Biomarker Based on Dual Signal Amplification Strategy of Graphene Sheets and Multi-Enzyme Functionalized Carbon Nanospheres

Dan Du[1,2], **Zhexiang Zou**[2], **Yongsoon Shin**[2], **Jun Wang**[2], **Hong Wu**[2], **Mark H. Engelhard**[2], **Jun Liu**[2], **Ilhan A. Aksay**[3], and **Yuehe Lin**[*,2]

[1] Key Laboratory of Pesticide and Chemical Biology of Ministry of Education, College of Chemistry, Central China Normal University, Wuhan 430079, PR China

[2] Pacific Northwest National Laboratory, Richland, WA 99352

[3] Department of Chemical Engineering, Princeton University, Princeton, NJ 08544

Abstract

A novel electrochemical immunosensor for sensitive detection of cancer biomarker α-fetoprotein (AFP) is described that uses a graphene sheet sensor platform and functionalized carbon nanospheres (CNSs) labeling with horseradish peroxidase-secondary antibodies (HRP-Ab2). Greatly enhanced sensitivity for the cancer biomarker is based on a dual signal amplification strategy: first, the synthesized CNSs yielded a homogeneous and narrow size distribution, which allowed several binding events of HRP-Ab2 on each nanosphere. Enhanced sensitivity was achieved by introducing the multi-bioconjugates of HRP-Ab2-CNSs onto the electrode surface through “sandwich” immunoreactions. Secondly, functionalized graphene sheets used for the biosensor platform increased the surface area to capture a large amount of primary antibodies (Ab1), thus amplifying the detection response. On the basis of the dual signal amplification strategy of graphene sheets and the multi-enzyme labeling, the developed immunosensor showed a 7-fold increase in detection signal compared to the immunosensor without graphene modification and CNSs labeling. The proposed method could respond to 0.02 ng mL^{-1} AFP with a linear calibration range from 0.05 to 6 ng mL^{-1}. This amplification strategy is a promising platform for clinical screening of cancer biomarkers and point-of-care diagnostics.

Sensitive detection of disease-related proteins is critical to many areas of modern biochemical and biomedical research. In particular, the clinical measurement of cancer biomarkers shows great promise for early disease detection and highly reliable predictions.[1,2] It also offers opportunities for understanding fundamental biological processes involved in disease progression and monitoring patient responses to therapy methods.[3] Conventional immunoassay methods, including the enzyme-linked immunosorbent assay (ELISA),[4,5] radioimmunoassay,[6,7] fluorescence immunoassay,[8,9] chemiluminescence assay,[10,11] electrophoretic immunoassay,[12] mass spectrometric immunoassay,[13,14] and immune-polymerase chain reaction (PCR) assay [15] allow reliable predictions. However, the increasing demand for early and ultrasensitive screening of cancer biomarkers is pushing the enhancement of detection sensitivity by signal amplification or novel detection technologies.[16-18] For point-of-care applications, the sensors need to be inexpensive, operationally simple, and highly sensitive to address both levels of the biomarkers in normal and cancer patient serums.

[*] To whom correspondence should be addressed. yuehe.lin@pnl.gov.

The electrochemical immunoassay combined with nano-structured materials opens new horizons for highly sensitive detection of biomarkers because of the nanoparticle-based signal amplification platform.[19,20] To date, three approaches have been developed for signal amplification of nanoparticle-based electrochemical biosensors: (1) Metal and semiconductor nanoparticles are directly used as electroactive labels to amplify the electrochemical response of DNA or proteins.[21-24] (2) Nanoparticles are used as carriers to load a large amount of electroactive species, such as ferrocene, to amplify the detection of biomolecules.[25-29] Our group has reported this novel strategy using poly (guanine)-functionalized silica nanoparticles to introduce a large amount of guanine residues on the electrode. Ru(bpy)-induced catalytic oxidation of guanine resulted in great enhancement of the anodic current.[25-27] (3) Enzyme-functionalized nanoparticles are used as the label to enhance detection sensitivity, which is obtained by increasing the enzyme loading toward a sandwich immunological reaction event.[30-33] Rusling's group has achieved greatly enhanced sensitivity by using bioconjugates featuring horseradish peroxidase (HRP) labels and secondary antibodies linked to carbon nanotubes (CNTs) for immunodetection of the prostate specific antigen.[30] Also, they developed an ultrasensitive immunosensor for a cancer biomarker by synthesizing magnetic bioconjugate particles containing 7500 HRP labels along with detection antibodies.[31] Recently, Liu and co-workers reported HRP-functionalized silica nanoparticles as a label for detecting α-fetoprotein (AFP).[32] The improved particle synthesis using a “seed-particles growth” route yielded particles of narrow size distribution, which allowed consistent loading of HRP and AFP antibodies to enhance detection sensitivity.

Carbon nanomaterials have attracted considerable attention in electrochemical biosensors because of their extraordinary physical properties and remarkable conductivities.[34,35] While CNTs have been widely used as labeling particles in immunoassays with excellent sensitivity, problems that need to be overcome include nanotube heterogeneity and purity. Recently, porous carbon nanospheres (CNSs) have also displayed unique advantages owing to the tenability of particle size and shape as well as the resident porosity that promotes diffusion of guest molecules through interconnected micropores.[36,37] A “green” synthetic approach has been developed that involves the transformation of sugars into homogeneous and stable colloidal CNSs, which are hydrophilic.[37,38] Such surface-functionalized CNSs and porous structures are potentially beneficial for labeling.

For carbon electrodes, the electrocatalytic properties strongly depend on their microstructure and surface chemistry. Recently, graphene has emerged as an interesting material because of its unusual electronic properties and large accessible surface area.[39,40] Biocompatible graphene sheets as a sensor platform not only present an abundant domain for bimolecular binding, but also play a role of fast electron-transfer kinetics and further signal amplification in electrochemical detection. [41-44] For example, a novel electrode system using reduced graphene oxide as a biosensing platform has been proposed. Graphene sheets showed favorable electrochemical activity to several electroactive compounds.[45] In addition, graphene electrodes exhibited a superior biosensing performance over single-walled carbon nanotubes toward dopamine detection in the presence of common interfering agents, such as ascorbic acid and serotonin.[46]

In this paper, we report an electrochemical immunosensor for sensitive detection of biomarkers based on a dual amplification mechanism resulting from multi-enzyme-antibody functionalized CNSs and functionalized graphene sheets as the sensor platform. The synthesized colloidal CNSs from fructose under hydrothermal treatment were employed as a carrier for HRP-secondary antibody (HRP-Ab2) immobilization. Greatly amplified sensitivity was achieved by loading a large number of enzymes. The modified screen-printed carbon electrode with functionalized graphene sheets was employed to attach the primary

antibody. AFP is a major plasma protein produced by the yolk sac and the liver. The AFP expression is often associated with hepatoma and teratoma and has been widely used as a diagnostic biomarker for hepatocellular carcinoma.[47] Here we used AFP as a model cancer biomarker and demonstrated the amplification process in sandwich detection. The proposed immunosensor shows potential applications in clinical screening of cancer biomarkers and point-of-care diagnostics.

Experimental Section

Reagents and Materials

AFP, mouse monoclonal antibody to AFP (anti-AFP, Ab1), and HRP-labeled mouse monoclonal antibody to AFP (HRP-anti-AFP, HRP-Ab2) were purchased from Abcam, Inc. Bovine serum albumin (BSA), Tween-20, 1-ethyl-3-(3-dimethylaminopropyl) carbodiimide hydrochloride (EDC), N-hydroxysuccinimide (NHS), 3,3′,5,5′-tetramethylbenzidine (TMB), chitosan, phosphate buffer saline (PBS), and 2-(N-morpholino)ethanesulfonic acid (MES) were acquired from Sigma/Aldrich. The graphene used in our study was made by thermal exfoliation of graphite oxide, [48] which starts with the chemical oxidation of graphite flakes to increase the c-axis spacing from 0.34 nm to 0.7 nm. The resulting graphite oxide was split apart through rapid thermal expansion to yield single but wrinkled graphene sheets functionalized with hydroxyl and carboxylic groups. [43]

Apparatus

Electrochemical experiments, including cyclic voltammetry (CV) and square wave voltammetry (SWV), were performed with an electrochemical analyzer CHI 660A (CH Instruments, Austin, TX) connected to a personal computer. Disposable screen-printed carbon electrodes (SPCE) consisting of graphene sheets-chitosan modified working carbon electrodes (GS-CHI/SPCE), a carbon counter electrode, and an Ag/AgCl reference electrode were purchased from Alderon Biosciences, Inc. A sensor connector (Alderon Biosciences, Inc.) was used to connect the disposable SPCE to the CHI electrochemical analyzer. Dried carbon spheres were characterized by using field emission scanning electron microscopy (FE-SEM) JEOL-JSEM 633F. X-ray photoelectron spectroscopy (XPS) measurements were taken with a Physical Electronics Quantum 2000 Scanning Microprobe. This system uses a focused monochromatic aluminum Kα X-ray (1486.7 eV) source for excitation and a spherical section analyzer. A 100-W X-ray beam focused to a diameter of 100 μm was rastered over a 1.3-mm × 0.2-mm rectangle on the sample. The high-energy resolution data were collected using a pass energy of 46.95 eV. These conditions produced a full-width half-maximum of 0.98 eV for the Ag $3d_{5/2}$ line. The binding-energy scale was calibrated using Cu 2p3/2 at 932.62 ± 0.05 eV and Au 4f at 83.96 ± 0.05 eV.

Synthesis of Colloidal CNSs

Colloidal CNSs was synthesized from fructose in closed systems under hydrothermal conditions and characterized by 13C solid-state nuclear magnetic resonance (NMR), Fourier transform-infrared (FT-IR) spectra, and electron imaging studies (SEM and transmission electron microscopy [TEM]). [49, 50] Briefly, *in situ* Raman spectra to follow the initial dehydration of fructose to hydrothermal furaldehyde in a concentrated aqueous solution (2.5 M) were measured in real time in a pressurized optical cell (25 mL) at temperatures ranging from 120 to 140°C. A 777.8-nm excitation (90° scattering geometry) was used that effectively suppressed fluorescence from the solution as it began to turn yellow. Measured peak intensities were normalized with respect to the intensity of the incident probe laser. Spectra of 13C NMR were collected from a Chemagenetics spectrometer (500 MHz: solution) and a Chemagenetics spectrometer (300 MHz: solid). The samples were prepared by hydrothermal treatment of the solution in a steel cell at a specific temperature and for a

specific time, and then the reactions were quenched by lowering the temperature naturally. [49, 50] Scheme 1 displays the dehydration and carbonization process of fructose and the following enzyme-antibody-functionalization of CNSs.

Immobilization of HRP-Ab2 onto CNSs (HRP-Ab2-CNSs)

To generate carboxylic groups on the surface of CNSs, 10 mg CNSs was treated with a mixture of concentrated H_2SO_4, HNO_3, and distilled water (3:1:6) for 2 hours at room temperature. The resulting dispersion was washed repeatedly with water until the pH was ~7.0. After centrifugation at 13,000 rpm for 5 min, the functionalized CNSs were then mixed with 1 mL 400 mM EDC and 100 mM NHS in pH 5.2 MES buffer and activated for 30 min. The buffer wash was repeated to remove excessive EDC and NHS. Subsequently, the resulting functionalized CNSs were dispersed in 1.0 mL pH 7.4 PBS and sonicated for 5 min to obtain a homogeneous dispersion. Then, 20 μL HRP-Ab2 at 2.0 mg/mL was added to the dispersion and stirred overnight at room temperature. The reaction mixture was washed with PBS and centrifuged at 13,000 rpm for 5 minutes three times, and the supernatant was discarded. The resulting mixture was redispersed in 1.0 mL pH 7.4 PBS containing 3% BSA and stored at 4°C. The HRP-Ab2-CNSs dispersion is stable and can keep the enzyme activity for at least 3 weeks.

To determine the amount of active HRP in the dispersion, the mixture was reacted with HRP substrate TMB. The reaction product was read at 650 nm. This was compared to a standard curve constructed with pure HRP by an enzyme activity experiment. The concentration of active Ab2-HRP in the stock HRP-Ab2-CNSs dispersion was determined to be 3.07 μg/mL.

Fabrication of Functionalized Graphene Sheets Immunosensor

Functional graphene sheets (FGSs) were prepared through a thermal expansion process. The detailed synthesis process and the characterization of the FGSs used in this work have been reported elsewhere. [51] The suspension of graphene was first prepared by dispersing 0.5 mg graphene in 1 mL of 0.2% chitosan solution (pH 5.2). The mixture was sonicated 1 hour to obtain a homogeneous dispersion. Then a 5-μL suspension was cast on a pretreated working carbon electrode and dried at room temperature. To attach primary AFP antibodies, 10 μL of freshly prepared 400-mM EDC and 100-mM NHS were placed onto the GS-CHI/SPCE and washed off after 30 min. This was immediately followed by a 2-h incubation at 37°C with 20 μL of 0.5-mg/mL primary AFP antibodies (Ab1) in pH 7.4 PBS. After washing with 0.05% Tween-20 and PBS buffer, the Ab1/GS-CHI/SPCE was incubated in 3% BSA and PBS solution at 37°C for 1 hour to block excess active groups and nonspecific binding sites on the surface. The electrode was then washed with 0.05% Tween-20 and PBS buffer before use.

Immunoassay Procedure for Detection of AFP

A sandwich immunoassay was used for determination of AFP. (1) The immunosensor, Ab1/GS-CHI/SPCE, was incubated with 10 μL of a different concentration of AFP standard antigen at 37°C for 60 min, followed by washing with 0.05% Tween-20 and PBS buffer. (2) Next, the electrode (AFP/Ab1/GS-CHI/SPCE) was incubated with 10 μL of HRP-Ab2-CNSs dispersion at 37°C for 40 min, followed by washing with 0.05% Tween-20 and PBS buffer to remove the nonspecific adsorption of CNSs. (3) The immunosensor was then detected in 2 mM *o*-phenylenediamine (*o*-PD) and 4 mM H_2O_2.

Results and Discussion

Dual Signal Amplification Strategy Using Graphene and HRP-anti-AFP-CNSs

Scheme 2 displayed electrochemical immunoassay steps, including a traditional labeled protocol (A) and a signal amplification strategy using multi-enzyme-antibody labels (B) on graphene sheets. Herein we pursued graphene sheets and a multi-enzyme-antibody labeling strategy to enhance sensitivity. The secondary antibody is enzyme-labeled conjugate (HRP-Ab2), which serves as a signaling antibody in sandwiched immunodetection. To achieve an amplification signal, we use CNSs as a carrier to load a large number of HRP-Ab2, which results in loading more enzymes in the sandwiched immunoreactions. Ggreatly amplified response was achieved by using multi-bioconjugates of HRP-Ab2-CNSs to replace HRP-Ab2. The graphene sheets used as a sensor platform increased the surface area to capture a large amount of primary antibodies, thus amplifying the detection signal.

SEM Images of Synthesized CNSs

Figure 1 shows SEM images of the final product of CNSs. They demonstrate a homogeneous distribution with an average size of 400 nm in diameter (Figure 1A). Detailed magnified images of CNSs (Figure 1B) appeared smooth with a small porous structure. These monodispersed CNSs were vital for loading HRP-Ab1 on each nanosphere, which would influence the sensitivity and analytical performance of the resulting immunosensor.

XPS Analysis of Functionalized CNSs and HRP-Ab2-CNSs

Figure 2 displays XPS spectra of the original synthesized CNSs, acid treated CNSs, and HRP-Ab2-CNSs conjugate. One can see that both the original synthesized CNSs (curve a) and acid treated CNSs (curve b) showed the binding energy of the core electrons for the C_{1s} line at 284.8 eV from the C-H groups (Figure 2A). After treating with concentrated acid, the functionalization of the CNSs were confirmed by the significantly increased signal in the peak at 288.6 eV (curve b), which was attributed to the COOH unit.[52] These data indicated that successful acid treatment of CNSs has introduced more carboxylic groups on CNSs. Furthermore, a strong N_{1s} binding energy at 399.8 eV was observed on the HRP-Ab2-CNSs conjugate (curve c) as shown in Figure 2B, while no signal could be detected on the original synthesized CNSs (curve a) and acid treated CNSs (curve b). The N_{1s} core level spectra showed a typical binding energy of the amide nitrogen atoms (HN-C=O) coming from the function of antibodies, [53] indicating successful modification of CNSs to form the HRP-Ab2-CNSs conjugate.

Electrochemical Behaviors of the Immunosensors

As shown in Figure 3, the cyclic voltammogram of Ab1/GS-CHI/SPCE did not show any detectable signal in pH 7.4 PBS (curve a). Upon adding 2 mM *o*-PD and 4 mM H_2O_2 to the PBS buffer, the cyclic voltammogram of Ab1/GS-CHI/SPCE exhibited a pair of stable and well-defined redox peaks at -0.125 V and -0.152 V (curve b), which correspond to the electrochemical response of *o*-PD. When incubating the immnuosensor with 2 ng mL^{-1} AFP, no obvious change in signal was observed (data not shown). But after incubating with the HRP-Ab2 solution, the resulting HRP-Ab2/AFP/Ab1/GS-CHI/SPCE displayed a slight increase in catalytic reduction current (curve c) because of HRP on the electrode surface. However, when replacing HRP-Ab2 with HRP-Ab2-CNSs as a detection antibody, the electrocatalytic current at HRP-Ab2-CNSs/AFP/Ab1/GS-CHI/SPCE (curve d) increased significantly. It is not surprising that the multi-enzyme-antibody labeling strategy enhanced the detection signal more than the traditionally labeled HRP-Ab2.

The signal amplification was also confirmed by SWV measurement. As shown in Figure 4, a 3.5-fold increase in the catalytic current was observed at HRP-Ab2-CNSs/AFP/Ab1/GS-

CHI/SPCE (curve a) compared with HRP-Ab2/AFP/Ab1/GS-CHI/SPCE (curve b) since HRP-Ab2-CNSs as a detection antibody could introduce more HRP on the electrode surface. This phenomenon could also be seen even with oxidized CHI/SPCE without graphene modification. The catalytic current obtained from HRP-Ab2-CNSs (curve c) at AFP/Ab1/CHI/SPCE was 3.0-fold higher than that from HRP-Ab2 (curve d). The achieved amplification was mainly ascribed to the excessive enzyme present in the CNSs label when using HRP-Ab2-CNSs as a detection antibody. Furthermore, we explored the role of graphene sheets as a sensor platform. Compared to AFP/Ab1/CHI/SPCE and AFP/Ab1/GS-CHI/SPCE, the catalytic current increased from 3.13 μA (curve c) to 7.87 μA (curve a) when using HRP-Ab2-CNSs as a detection antibody. Also, the responses increased from 1.18 μA at AFP/Ab1/CHI/SPCE (curve d) to 2.66 μA at AFP/Ab1/GS-CHI/SPCE (curve b) when using traditionally labeled HRP-Ab2. These data illustrated that although CHI/SPCE could also specifically capture Ab1, much lower peak currents and slight positively shifted potentials were observed compared to those at GS-CHI/SPCE. The presence of graphene not only obviously increased the surface area to capture more antibodies on the electrode surface, but also accelerated electron transfer. Based on the dual amplification of graphene sheets and HRP-Ab2-CNSs, the catalytic current at HRP-Ab2-CNSs/AFP/Ab1/GS-CHI/SPCE enhanced about 7-fold in comparison with that at HRP-Ab2/AFP/Ab1/CHI/SPCE without graphene modification and CNSs labeling.

A series of control experiments were conducted in PBS containing *o*-PD and H_2O_2 by SWV measurements. As shown in Figure 5, both the Ab1/CHI/SPCE (a) and Ab1/GS-CHI/SPCE (b) presented small signals. A slight increase of catalytic currents was obtained when the Ab1/GS-CHI/SPCE was directly exposed to HRP-Ab2 (c) or HRP-Ab2-CNSs (e) without pre-incubation in an AFP solution. These responses might result from nonspecific adsorption on the electrode. However, after incubating with 2 ng mL^{-1} AFP, the responses of both obtained HRP-Ab2/AFP/Ab1/GS-CHI/SPCE (d) and HRP-Ab2-CNSs/AFP/Ab1/GS-CHI/SPCE (f) increased greatly. Although the incubation of HRP-Ab2-CNSs (e) showed a much higher background signal than that of HRP-Ab2 (c), the signal-to-noise ratio (S/N) before and after incubating with AFP from HRP-Ab2-CNSs (f/e) was much larger than that from HRP-Ab2 (d/c), thus amplifying the detection signal.

Optimization of Detection Conditions

The incubation time was an important parameter for both capturing AFP antigens and specifically recognizing HRP-Ab2-CNSs on the electrode surface. After increasing the incubation time with 2 ng mL^{-1} AFP, the SWV peak current at the HRP-Ab2-CNSs/AFP/Ab1/GS-CHI/SPCE increased and tended to a steady value after 60 min (curve a in Figure 6A), indicating a tendency to thoroughly capture AFP antigens on the electrode surface. After incubating the AFP/Ab1/GS-CHI/SPCE with HRP-Ab2-CNSs used in the second immunoassay incubation step, the SWV response increased and reached a plateau at 40 min (curve b in Figure 6A). A long time incubation could result in a large non-specific signal. Therefore, the optimal incubation time for the first and second immunoreactions was 60 min and 40 min, respectively.

The performance of the electrochemical enzyme-catalyzed analysis was related to the concentration of *o*-PD and H_2O_2 in the measuring system.[54] As shown in Figure 6B, the SWV peak current of the resulting HRP-Ab2-CNSs/AFP/Ab1/GS-CHI/SPCE increased with the increasing concentrations of *o*-PD (curve a) and H_2O_2 (curve b) and maintained the maximum value at higher concentrations. Afterward, the enzymatic reaction rate depended on the amount of the labeled HRP. This result suggested a Michaelis-Menten's mechanism in the electrochemical enzyme-catalyzed analysis. Therefore, the optimal *o*-PD and H_2O_2 concentrations were 2 mM and 4 mM, respectively.

Electrochemical Detection

Under optimal conditions, the electrocatalytic currents of the HRP-Ab2-CNSs/AFP/Ab1/GS-CHI/SPCE increased with the increase of AFP concentrations (Figure 7). The increase of the reduction current was proportional to the AFP concentration in the range of 0.05 to 6 ng mL^{-1}, and the linear regression equation was $i_p(\mu A) = 3.167c + 0.7367$ with a detection limit of 0.02 ng mL^{-1}. The detectable concentration of AFP in the present work was comparable to the detection limit reported by using other amplification methods, including 0.01 ng mL^{-1} using SiO_2 nanoparticles as a label [32] and lower than 1 ng mL^{-1} on carboxylic resin beads.[55] Since the threshold of AFP in human serum was 10 ng mL^{-1}, [56] a high concentration of AFP in the serum needs to be diluted within the detection dynamic range.

To further investigate the selectivity of the proposed immunosensor for AFP detection, the immunosensor was incubated in 2 ng mL^{-1} AFP containing a different interfering agent, such as carcinoembryonic antigen (CEA), carcinoma antigen 125 (CA125), and a prostate-specific antigen (PSA). No remarkable change of current was observed in comparison with the result obtained in the presence of AFP only, indicating good selectivity of the proposed AFP immunosensor.

Evaluation of the Immunosensor

The accuracy of the quantification of AFP was tested by adding different amounts of AFP into serum samples, and the results were compared with ELISA. The results are summarized in Table 1. The recoveries from these two methods ranged from 97.1 to 104.6% and 97.4 to 103.8%, respectively. The relative deviation was lower than 3.0%, indicating acceptable accuracy.

The reproducibility of the proposed immunosensor was evaluated by intra- and inter-assay coefficients of variation (CVs). The intra-assay precision of the analytical method was evaluated by analyzing one immunosensor for six replicate determinations. The CVs of the intra-assay were 3.5% and 5.9% at 0.1 and 2.0 ng mL^{-1} AFP, respectively. Similarly, the inter-assay CVs on six immunosensors were 4.3% and 5.5% at 0.1 and 2.0 ng mL^{-1} AFP, respectively. These results indicated acceptable reproducibility and precision of the proposed immunosensor.

Conclusions

In this work, we have successfully developed a highly sensitive and selective immunosensor for detecting cancer biomarkers and demonstrated this signal amplification procedure. The greatly enhanced sensitivity relies upon a dual signal-amplification scheme: (1) CNSs as the enzyme-loading carrier can load many enzyme molecules on each CNSs. The labeling protocol allows multiple signals per binding event provided by using HRP-Ab2-CNSs in place of conventional HRP-Ab2, and (2) graphene sheets can provide a high density of primary antibodies because of their high surface area. The resulting immunosensor possess high sensitivity, good reproducibility, and cost-effective analytical performance. We anticipate that this method can be expanded readily for detecting other relevant biomarkers and has the potential for reliable point-of-care diagnostics of cancer and other diseases.

Acknowledgments

The work was done at Pacific Northwest National Laboratory (PNNL) and was supported partially by Grant U54 ES16015 from the National Institute of Environmental Health Sciences, the National Institutes of Health, and a PNNL Laboratory Directed Research and Development project. This work was also supported partially by the National Natural Science Foundation of China (20705010). PNNL is operated for the U.S. Department of Energy (DOE) by Battelle under Contract DE-AC05-76RL01830. The characterization was performed using EMSL, a national scientific user facility sponsored by the Department of Energy's Office of Biological and Environmental

Research and located at Pacific Northwest National Laboratory. IAA acknowledges support from ARO/MURI under grant number W911NF-04-1-0170.

References

1. Kitano H. Science 2002;295:1662–1664. [PubMed: 11872829]
2. Srinivas PR, Kramer BS, Srivastava S. Lancet Oncol 2001;2:698–704. [PubMed: 11902541]
3. Wilson MS, Nie WY. Anal Chem 2006;78:6476–6483. [PubMed: 16970323]
4. Voller A, Bartlett A, Bidwell DE. J Clin Pathol 1978;31:507–520. [PubMed: 78929]
5. Yates AM, Elvin SJ, Williamson DE. J Immunoassay 1999;20:31–44. [PubMed: 10225513]
6. Goldsmith S. J Semin Nucl Med 1975;5:125–152.
7. Teppo AM, Maury CP. J Clin Chem 1987;33:2024–2027.
8. Matsuya T, Tashiro S, Hoshino N, Shibata N, Nagasaki Y, Kataoka K. Anal Chem 2003;75:6124–6132. [PubMed: 14615991]
9. Cesaro-Tadic S, Dernick G, Juncker D, Buurman G, Kropshofer H, Michel B, Fattinger C, Delamarche E. Lab Chip 2004;4:563–569. [PubMed: 15570366]
10. Fu ZF, Hao C, Fei X, Ju HX. J Immunol Methods 2006;312:61–67. [PubMed: 16647079]
11. Fu ZF, Yan F, Liu H, Yang ZJ, Ju HX. Biosens Bioelectron 2008;23:1063–1069. [PubMed: 18068971]
12. Schmalzing D, Nashabeh W. Electrophoresis 1997;18:2184–2193. [PubMed: 9456033]
13. Niederkofler EE, Tubbs KA, Gruber K, Nedelkov D, Kiernan UA, Williams P, Nelson RW. Anal Chem 2001;73:3294–3299. [PubMed: 11476228]
14. Hu SH, Zhang SC, Hu ZC, Xing Z, Zhang XR. Anal Chem 2007;79:923–929. [PubMed: 17263317]
15. Saito K, Kobayashi D, Sasaki M, Araake H, Kida T, Yagihashi A, Yajima T, Kameshima H, Watanabe N. Clin Chem 1999;45:665–669. [PubMed: 10222353]
16. Polsky R, Gill R, Kaganovsky L, Willner I. Anal Chem 2006;78:2268–2271. [PubMed: 16579607]
17. Bao YP, Wei TF, Lefebvre PA, An H, He LX, Kunkel GT, Müller UR. Anal Chem 2006;78:2055–2059. [PubMed: 16536446]
18. Liu GD, Wang J, Wu H, Lin YH. Anal Chem 2006;78:7417–7423. [PubMed: 17073407]
19. Daniel MC, Astruc D. Chem Rev 2004;104:293–346. [PubMed: 14719978]
20. Liu G, Lin Y. Talanta 2007;74:308–317. [PubMed: 18371644]
21. Hazarika P, Ceyhan B, Niemeyer CM. Small 2005;1:844–848. [PubMed: 17193537]
22. Wang J, Xu D, Kawde AN, Polsky R. Anal Chem 2001;73:5576–5581. [PubMed: 11816590]
23. Authier L, Grossiord C, Brossier P, Limoges B. Anal Chem 2001;73:4450–4456. [PubMed: 11575792]
24. Liu GD, Lin YH. J Am Chem Soc 2007;129:10394–10401. [PubMed: 17676734]
25. Wang J, Liu GD, Engelhard MH, Lin YH. Anal Chem 2006;78:6974–6979. [PubMed: 17007523]
26. Wang J, Liu GD, Lin YH. Small 2006;2:1134–1138. [PubMed: 17193577]
27. Wang J, Liu G, Wu H, Lin YH. Anal Chim Acta 2008;610:112–118. [PubMed: 18267147]
28. Cui R, Liu C, Shen J, Gao D, Zhu JJ, Chen HY. Adv Funct Mater 2008;18:2197–2204.
29. Jie G, Huang H, Sun X, Zhu JJ. Biosens Bioelectron 2008;23:1896–1899. [PubMed: 18406128]
30. Yu X, Munge B, Patel Y, Jensen G, Bhirde A, Gong JD, Kim SN, Gillespie J, Gutkind JS, Papadimitrakopoulos F, Rusling JF. J Am Chem Soc 2006;128:11199–11205. [PubMed: 16925438]
31. Mani V, Chikkaveeraiah BV, Patel V, Silvio Gutkind J, Rusling JF. ACS Nano 2009;3:585–594. [PubMed: 19216571]
32. Wu YF, Chen CL, Liu SQ. Anal Chem 2009;81:1600–1607. [PubMed: 19140671]
33. Zhong ZY, Li MX, Xiang DB, Dai N, Qing Y, Wang D, Tang DP. Biosens Bioelectron 2009;24:2246–2249. [PubMed: 18977130]
34. McCreery RL. Chem Rev 2008;108:2646. [PubMed: 18557655]

35. Katz E, Willner I. Chem Phys Chem 2004;5:1084. [PubMed: 15446731]
36. Wang HT, Holmberg BA, Yan YS. J Mater Chem 2002;12:3640–3643.
37. Sun X, Li Y. Angew Chem Int Ed 2004;43:597–601.
38. Feather MS, Harris JF. Adv Carbohydr Chem Biochem 1973;28:161–224.
39. Shang NG, Papakonstantinou P, McMullan M, Chu M, Stamboulis A, Potenza A, Dhesi SS, Marchetto H. Adv Funct Mater 2008;18:3506.
40. Tang LH, Wang Y, Li YM, Feng HB, Lu J, Li JH. Adv Funct Mater 2009;19:1–8.
41. Wang Y, Lu J, Tang LH, Chang HX, Li JH. Anal Chem 2009;81:9710–9715. [PubMed: 19902903]
42. Li YM, Tang LH, Li JH. Electrochem Commun 2009;11:846–849.
43. Kang XH, Wang J, Kang XH, Wu H, Aksay IA, Liu J, Lin YH. Biosens Bioelectron 2009;25:901–905. [PubMed: 19800781]
44. Shan CS, Yang HF, Song JF, Han DX, Ivaska A, Niu L. Anal Chem 2009;81:2378–2382. [PubMed: 19227979]
45. Zhou M, Zhai YM, Dong SJ. Anal Chem 2009;81:5603–5613. [PubMed: 19522529]
46. Alwarappan S, Erdem A, Liu C, Li CZ. J Phys Chem C 2009;113:8853–8857.
47. Tamura Y, Yamagiwa S, Aoki Y, Kurita S, Suda T, Ohkoshi S, Nomoto M, Aoyagi Y. Dig Dis Sci 2009;54:2530–2537. [PubMed: 19093203]
48. Schniepp HC, Li JL, McAllister MJ, Sai H, Herrera-Alonso M, Adamson DH, Prud'homme RK, Car R, Saville DA, Aksay IA. J Phys Chem B 2006;110:8535–8539. [PubMed: 16640401]
49. Shin YS, Wang LQ, Bae IT, Arey BW, Exarhos GJ. J Phys Chem C 2008;112:14236–14240.
50. Yao C, Shin YS, Wang LQ, Windisch CF, Samuels WD, Arey BW, Wang CM, Risen WM Jr, Exarhos GJ. J Phys Chem C 2007;111:15141–15145.
51. a) Schniepp HC, Li JL, McAllister MJ, Sai H, Herrera-Alonso M, Adamson DH, Prud'homme RK, Car R, Saville DA, Aksay IA. J Phys Chem B 2006;110:8535–8539. [PubMed: 16640401] b) McAllister MJ, Li JL, Adamson DH, Schniepp HC, Abdala AA, Liu J, Herrera-Alonso M, Milius DL, Car R, Prud'homme RK, Aksay IA. Chem Mater 2007;19:4396–4404.
52. Shen G, Anand MFG, Levicky R. Nucleic Acids Res 2004;32:5973–5980. [PubMed: 15537837]
53. Darain F, Gan KL, Tjin SC. Biomed Microdevices 2009;11:653–661. [PubMed: 19130240]
54. Chen W, Ding L, Lei JP, Ding SJ, Ju HX. Anal Chem 2008;80:3867–3872. [PubMed: 18407618]
55. Yang Z, Fu Z, Yan F, Liu H, Ju HX. Biosens Bioelectron 2008;24:35–40. [PubMed: 18430562]
56. Wu J, Fu ZF, Yan F, Ju HX. Trends in Anal Chem 2007;7:679–688.

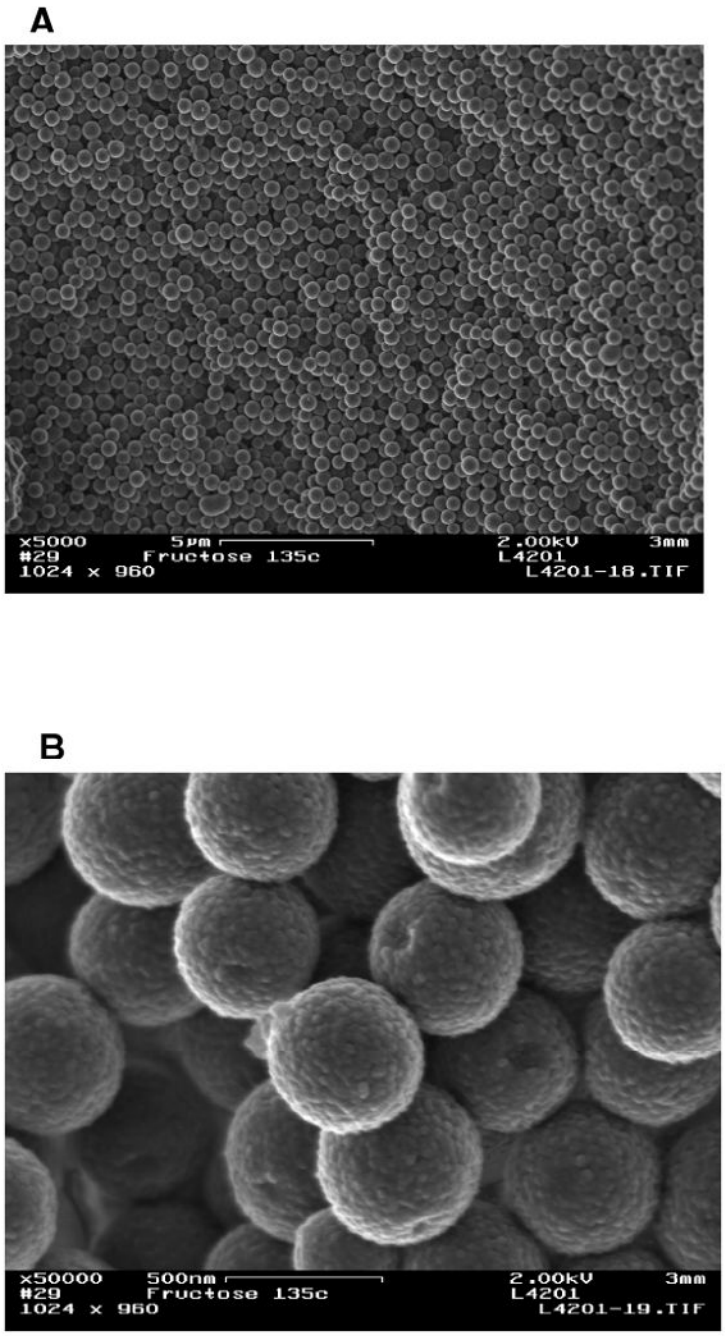

Figure 1.
SEM images of carbon nanospheres with 5000 (A) and 50,000 (B) magnification.

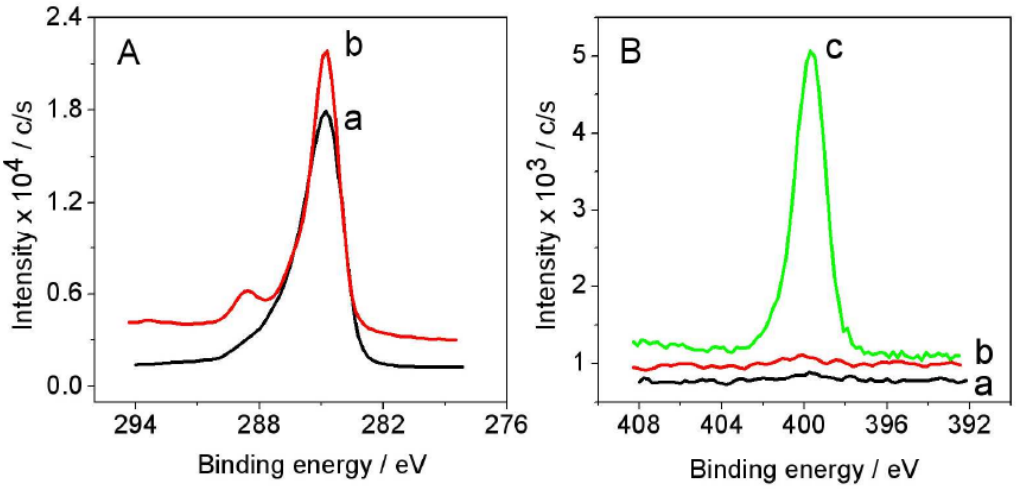

Figure 2.
XPS measurements of C_{1s} (A) and N_{1s} (B) from the synthesized CNSs (a), acid treated CNSs (b), and HRP-Ab2-CNSs conjugate (c).

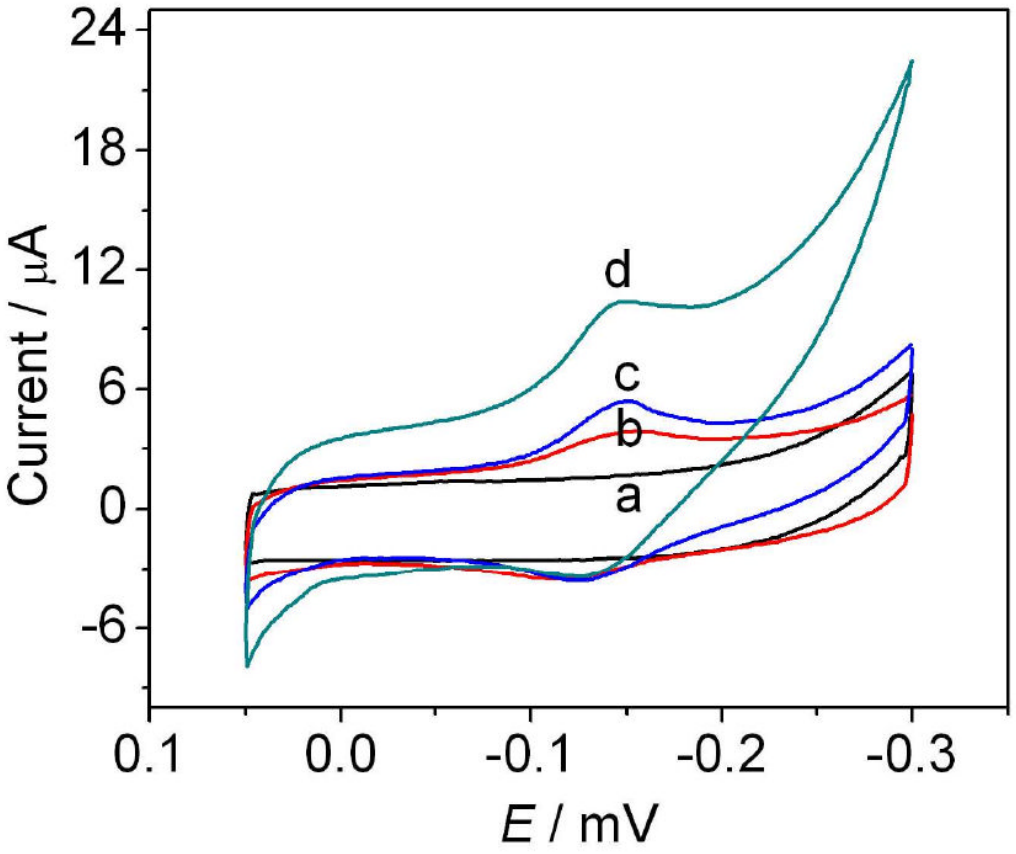

Figure 3.

Cyclic voltammograms of Ab1/GS-CHI/SPCE in pH 7.4 PBS (a) and Ab1/GS-CHI/SPCE (b), HRP-Ab2/AFP/Ab1/GS-CHI/SPCE (c) and HRP-Ab2-CNSs/AFP/Ab1/GS-CHI/SPCE (d) in PBS containing 2 mM o-PD and 4 mM H_2O_2. 2 ng mL^{-1} AFP was used during the incubation process at 37°C for 1 hour.

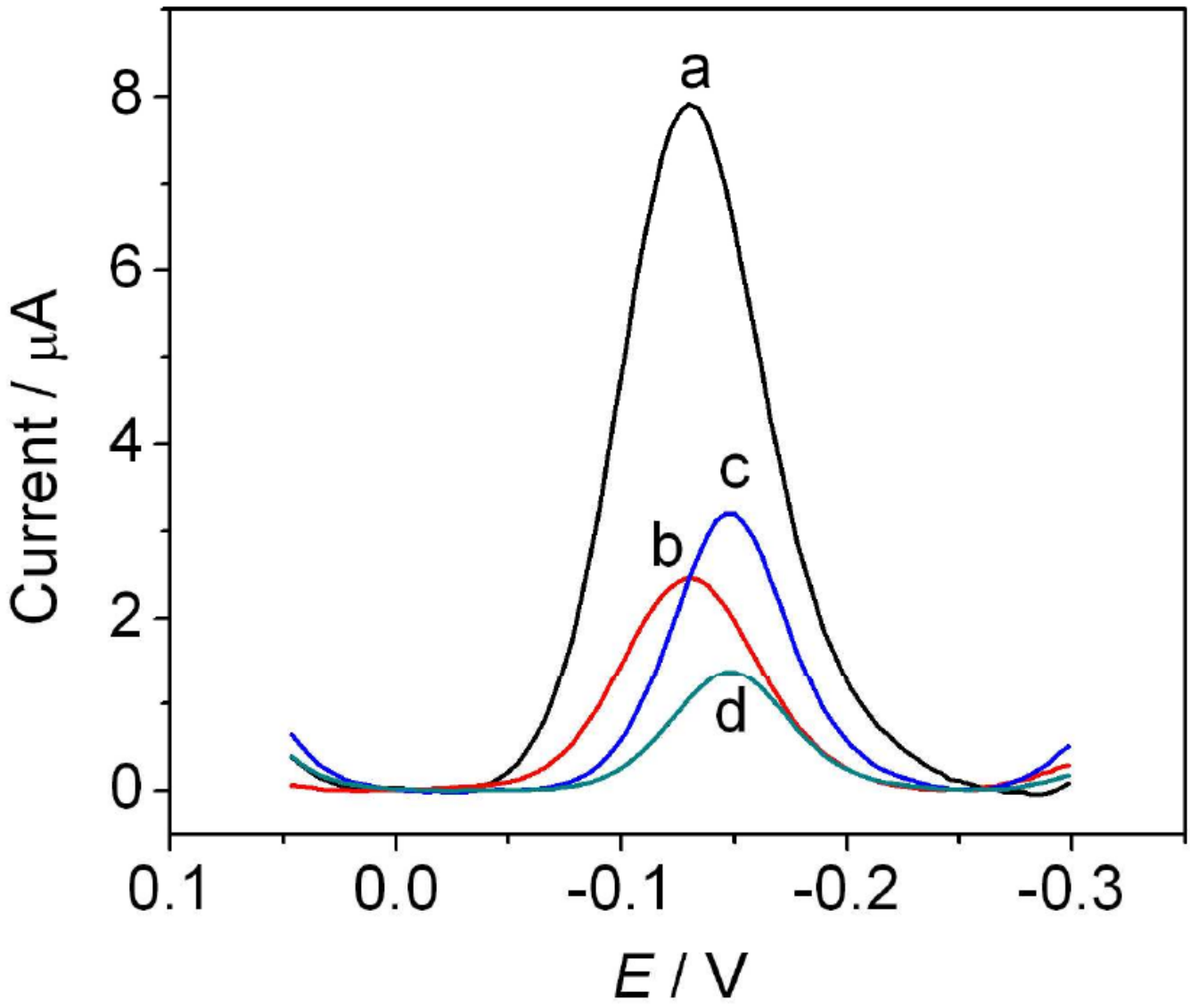

Figure 4.

Square wave voltammograms of HRP-Ab2-CNSs/AFP/Ab1/GS-CHI/SPCE (a), HRP-Ab2/AFP/Ab1/GS-CHI/SPCE (b), HRP-Ab2-CNSs/AFP/Ab1/CHI/SPCE (c), and HRP-Ab2/AFP/Ab1/CHI/SPCE (d) in pH 7.4 PBS containing 2 mM o-PD and 4 mM H_2O_2. Two nanograms mL^{-1} AFP was used during the incubation process at 37°C for 1 h.

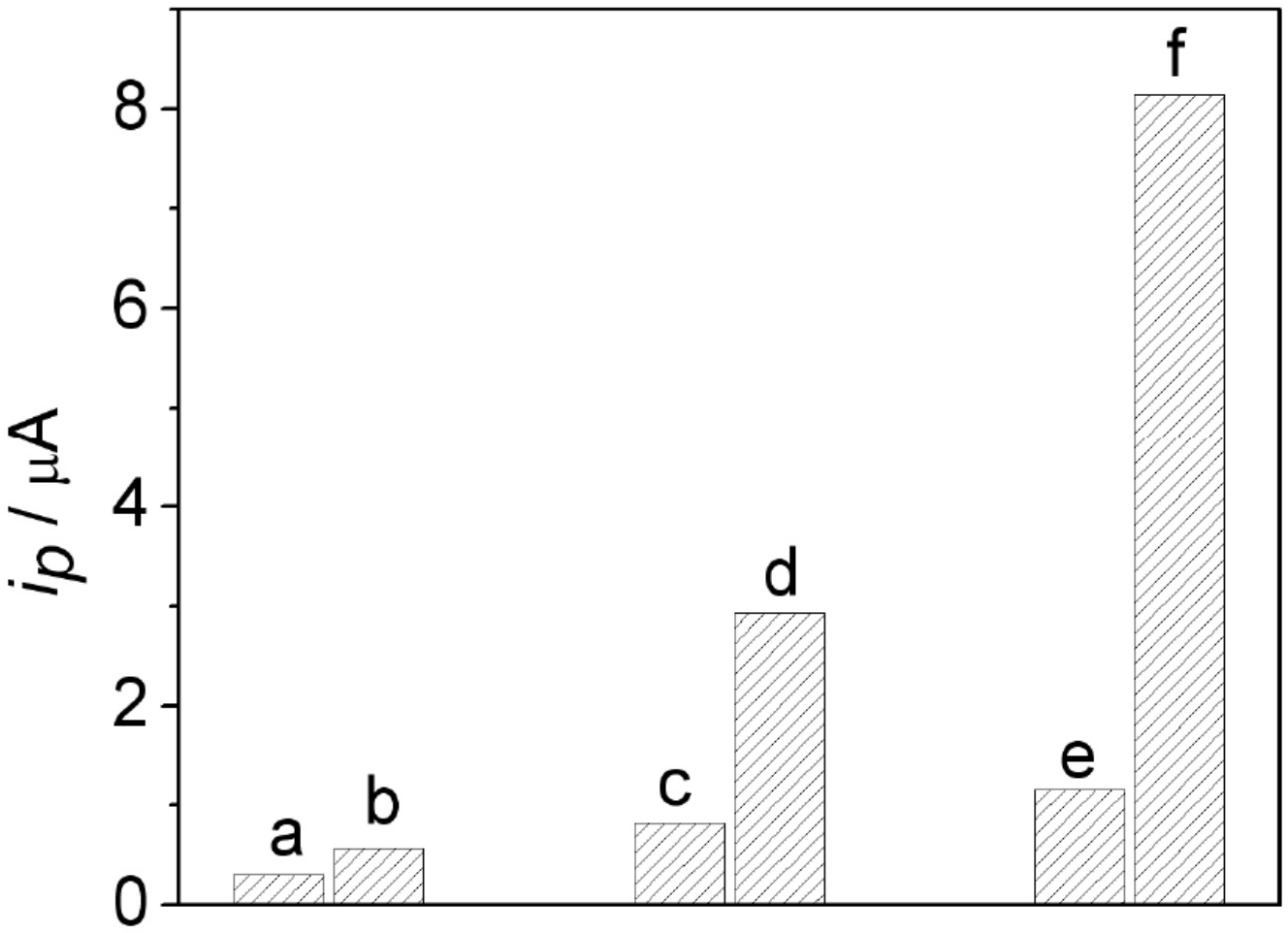

Figure 5.

Amperometric responses of Ab1/CHI/SPCE (a), Ab1/GS-CHI/SPCE (b), HRP-Ab2/Ab1/Ab1/GS-CHI/SPCE (c), HRP-Ab2/AFP/Ab1/GS-CHI/SPCE (d), HRP-Ab2-CNSs/Ab1/GS-CHI/SPCE (e), and HRP-Ab2-CNSs/AFP/Ab1/GS-CHI/SPCE (f) in pH 7.4 PBS containing 2 mM o-PD and 4 mM H_2O_2.

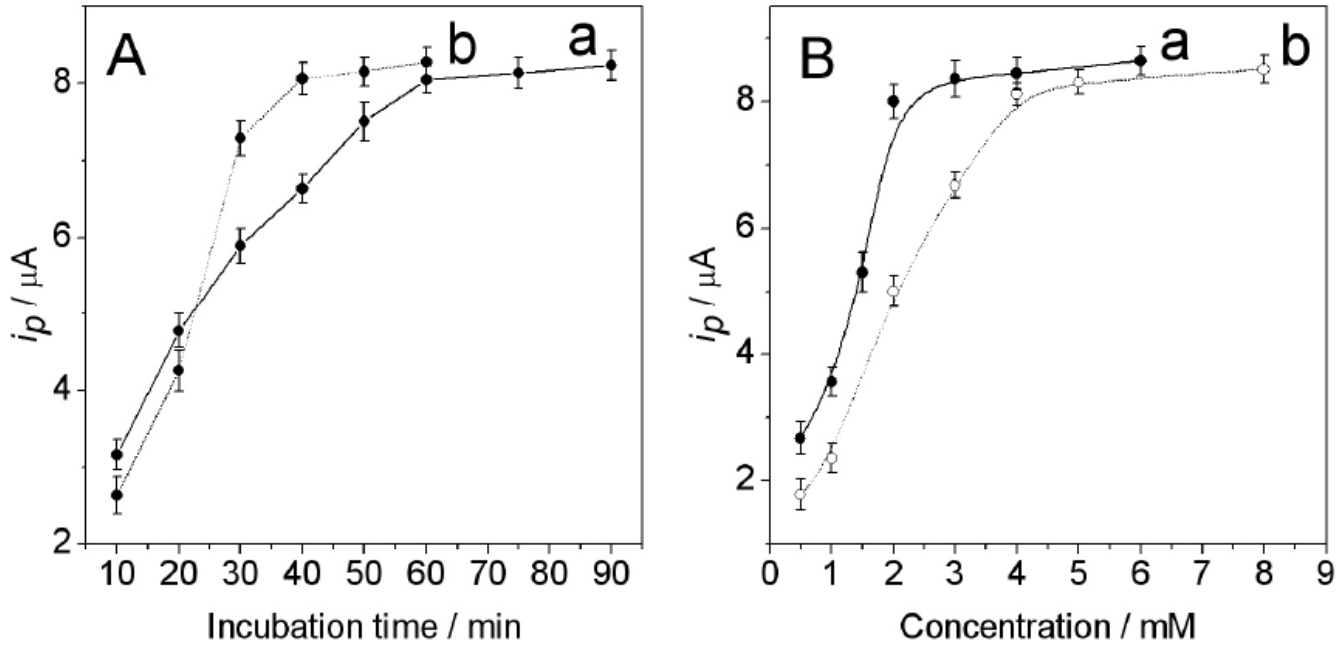

Figure 6.

(A) Dependence of SWV peak currents on the incubation time of AFP (a) and HRP-Ab2-CNSs (b) at Ab1/GS-CHI/SPCE. (B) Dependence of SWV peak currents on concentrations of o-PD (a) and H_2O_2 (b).

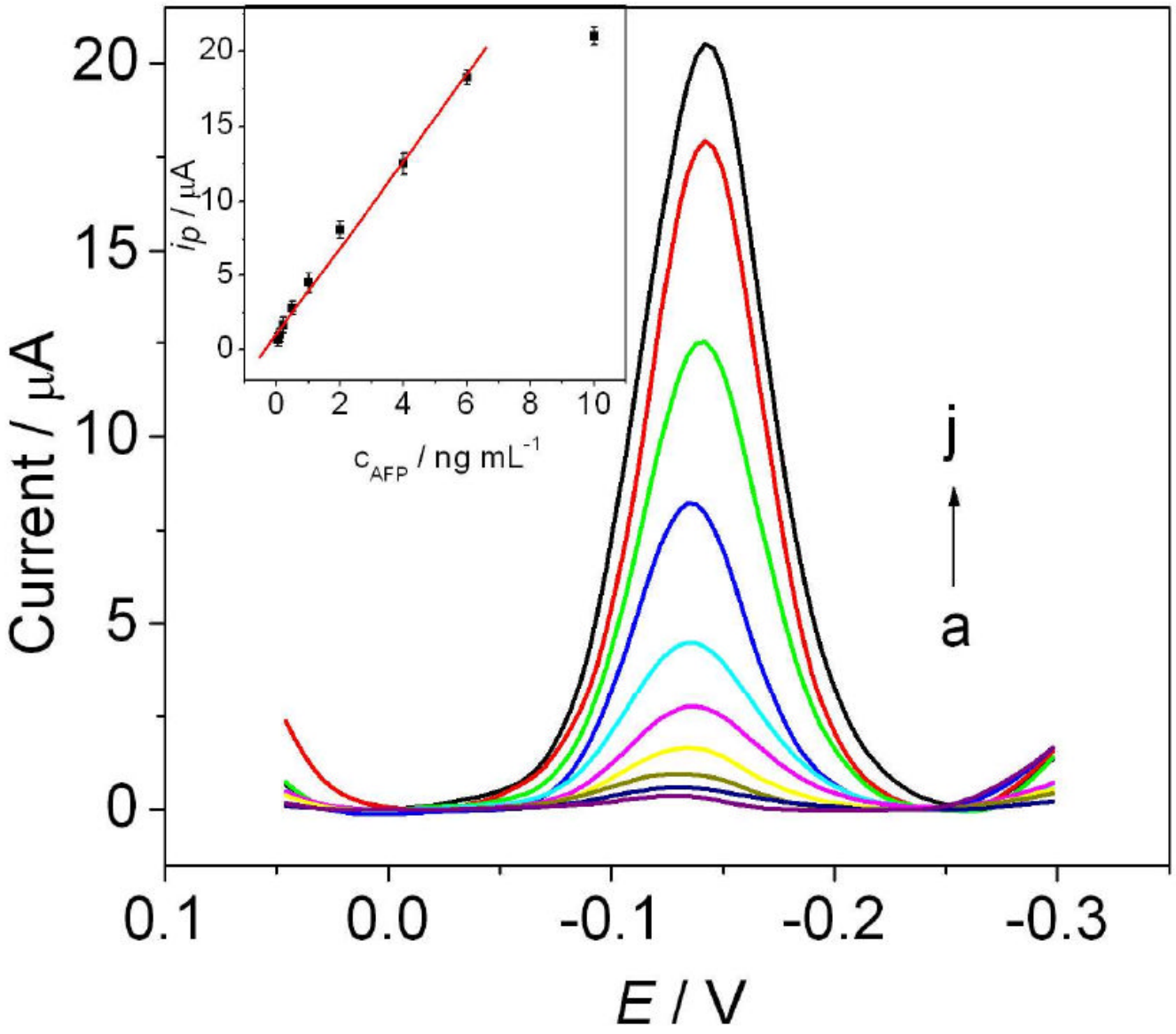

Figure 7.
SWV curves of HRP-Ab2-CNSs/AFP/Ab1/GS-CHI/SPCE after incubation with 0 (a), 0.05 (b), 0.1 (c), 0.2 (d), 0.5 (e), 1 (f), 2 (g), 4 (h), 6 (i), and 10 (j) ng mL^{-1} AFP in pH 7.4 PBS containing 2 mM o-PD and 4 mM H_2O_2. Inset: plot of the electrocatalytic currents of the immunosensor vs the concentrations of AFP.

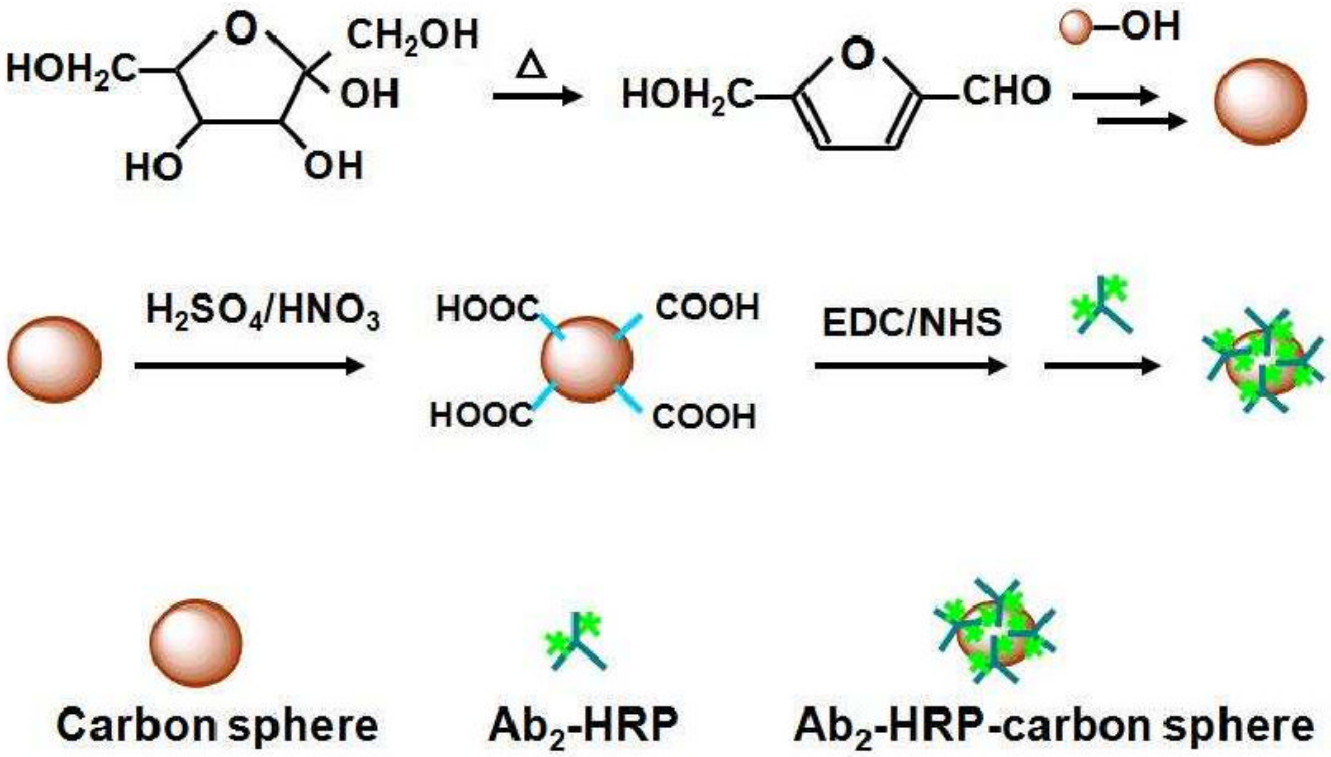

Scheme 1.
Schematic illustration of the dehydration and carbonization process of fructose and the following enzyme-antibody-functionalized CNSs.

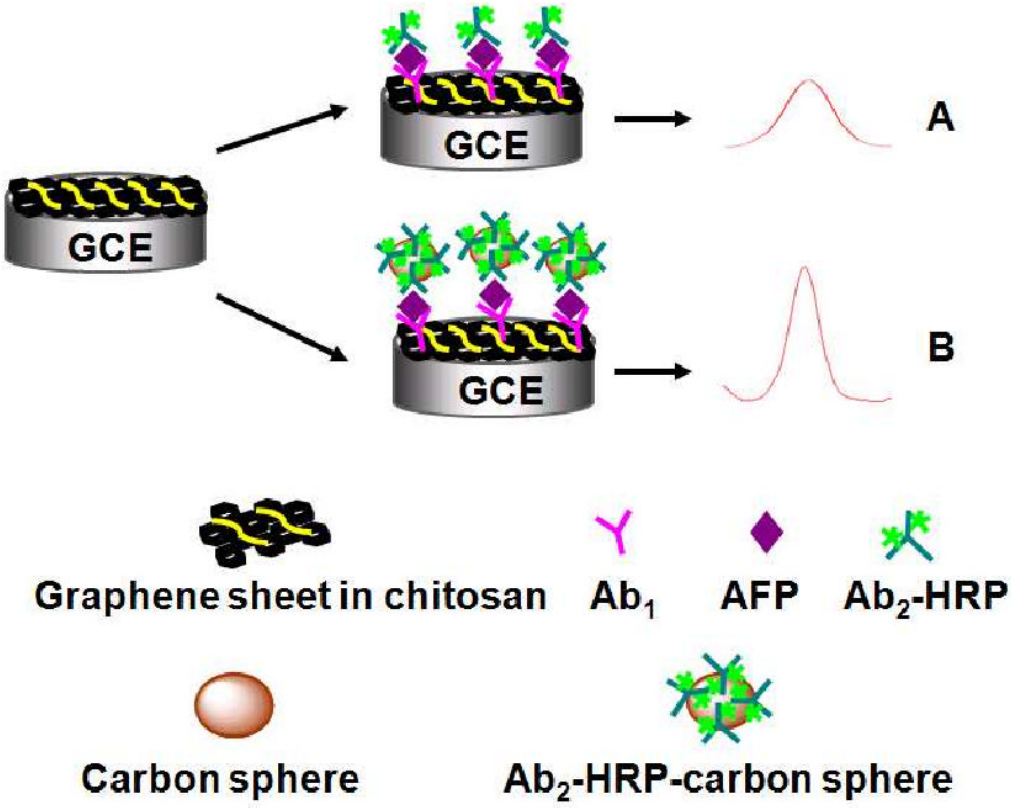

Scheme 2.

Schematic illustration of the detection principles of HRP-Ab2/AFP/Ab1/GS-CHI/SPCE (A) and HRP-Ab2-CNSs/AFP/Ab1/GS-CHI/SPCE (B) using a signal amplification strategy at the graphene sheets sensor platform.

Table 1

Recovery Studies of AFP in Serum Samples with Two Methods

Sample	Immunosensor concentrations (ng mL^{-1})		Immunosensor recoveries (%)	ELISA concentrations (ng mL^{-1})		ELISA recoveries (%)	Relative deviation (%)
	Added	Found		Added	Found		
1	0.5	0.523	104.6	0.5	0.519	103.8	0.77
2	1.0	0.971	97.1	1.0	0.974	97.4	-0.31
3	2.0	1.986	99.3	2.0	2.021	101.1	-1.73
4	3.0	2.933	97.8	3.0	3.017	100.6	-2.78